

Deliverable D3.5

Report on defect detection and classification algorithm for DED-LB

Funded by the European Union. Views and opinions expressed are however those of the author(s) only and do not necessarily reflect those of the European Union. Neither the European Union nor the granting authority can be held responsible for them.



Action number: #101138859

Action Acronym: DILAPRO
Action Name: Digital Laser Production

Deliverable Due date: 30/06/2025
Deliverable hand-in date: 31/07/2025

Revision	Date	Author/Organisation	Description
01	24-07-2025	Karl SOFINOWSKI, CRM Group	Initial full draft
02	29-07-2025	Karl SOFINOWSKI, CRM Group	Integrated comments from partners

Copyright © by DILAPRO All Rights Reserved

Table of contents

Executive Summary **3**

1. Introduction **4**

2. Defect Detection Approach **5**

2.1 Off-line data acquisition 5

2.1.1 Thermal camera 6

2.1.2 Laser power and profile monitor 7

2.1.3 Ambient temperature and humidity detector 7

2.2 On-line data acquisition 8

2.2.1 CLAMIR infrared camera 8

2.2.2 Coaxial pyrometer 9

2.2.3 2D profilometer 9

2.2.4 Eddy Current sensor (Prima Additive) 10

2.3 Defect labeling 12

2.3.1 Gas pores 12

2.3.2 Lack of fusion 13

2.3.3 Cracks 13

2.3.4 Thermal distortion and warpage 13

2.3.5 Layer height and surface quality (roughness and waviness) 13

2.4 Demonstration of closed-loop control 14

3. Construction of Machine Learning Dataset **16**

3.1 Live sensor data 18

4. Classification Algorithm **21**

4.1 Criteria for defect classification 22

4.2 Model Training and Selection Criteria 22

5. Conclusion **23**

6. References **24**

Copyright © by DILAPRO All Rights Reserved | D3.5 - Report on defect detection and classification algorithm for DED-LB

Executive Summary

Work Package 3 (WP3) of project DILAPRO deals with monitoring and quality control processes to improve and validate sensor data for creating a digital twin. Within this framework, Deliverable D3.5 presents the ongoing development of a defect detection and classification algorithm for DED-LB additive manufacturing.

Building on the technical solutions presented in Deliverable D3.1 [1], five primary sensors have been identified and integrated into the DED systems at CRM Group and Prima Additive. The sensors and their roles in defect detection are:

- **Coaxial pyrometer :** On-line measurement of temperature at the center of melt pool. Used for prediction of gas porosity, lack of fusion defects, and layer quality.
- **Infrared thermal camera :** Off-line measurement of the temperature evolution at the surface of the build. Used for measuring thermal gradients to predict internal stress development, warpage and thermal distortion, and cracking.
- **2D profilometer** : On- and off-line measurement of the build geometry. Used for monitoring and closed-loop correction of layer height and quality fluctuations; used for off-line measurement of final build dimensions.
- **Eddy current sensor :** On-line measurement of internal defect development. Used for direct measurement of gas porosity, lack of fusion defects, and internal cracks.

The following sensors are still being integrated into the machine:

- **CLAMIR coaxial infrared camera :** On-line measurement of melt pool size and profile. Will be used for monitoring and closed-loop correction of internal defect generation.

To create the feedback controls for the sensors, a machine learning model is being developed that will identify key relationships between process parameters and defects. The regression algorithms and performance of the models will be evaluated using the same methodology as described in Deliverable D3.3 [2].

To train the model, a dataset of 256 distinct Inconel 718 samples has been produced at CRM by varying laser spot size, scan speed, laser power, and line overlap. Data from the pyrometer, off-line infrared camera, and 2D profilometer will be used as inputs to the model. The objective of the model is to predict the sigmoid-transformed relative density of the Inconel 718 samples printed by DED. The best model will be selected based on criteria established in Deliverable D3.3 [2], including predictive accuracy, performance consistency, and lower bound of true performance.

Copyright © by DILAPRO All Rights Reserved

1. Introduction

The DILAPRO project will improve additive manufacturing of complex products by creating a Digital Twin software. The software will be used for the digital certification of the manufactured part. The ultimate goal is to monitor the build conditions and produce a certified part without further necessary testing. The digital twin, created from the sensor history, will serve as the certification of part quality and conformity. DILAFACT software developed during the project will establish guidelines regarding the choice of technology, process parameters and print trajectory. DILACERT software will support the digital qualification of the part by monitoring the process parameters and the use of direct defect detection.

Six pilot lines are identified for the project, including three laser powder bed fusion (LPBF) machines, two direct energy deposition (DED) machines and one laser texturing machine.

The first step of work package 3, "WP3. Monitoring and Quality Control", was to identify and install the appropriate sensors for each pilot line. The results of the search were reported in Deliverable D3.1[1]. The second step of WP3 is to develop and validate a machine learning (ML) model to guide closed-loop control algorithms that will improve the stability and "first-time" reliability of the printing processes. The feedback from the sensors will be used simultaneously to ensure part quality and to act as input to the digital certificate of quality [3].

This Deliverable D3.5 "Report on defect detection and classification algorithm for DED-LB" deals with the defect detection approach for DED-LB technologies only. D3.5 builds on the work presented in Deliverable D3.4 [4], which focused on algorithm development for Laser Powder Bed Fusion (L-PBF) using exploratory machine learning approaches. Due to delays in reception and installation of the sensors, the printing of the training data set was delayed by approximately three months. The samples have been printed and they are currently being characterized to generate input for the ML model. Here, we present the selected sensors for DED-LB only, their role in defect identification, the printing of a DED-LB training dataset for the ML model, and its future development.

Copyright © by DILAPRO All Rights Reserved

2. Defect Detection Approach

2.1 Off-line data acquisition

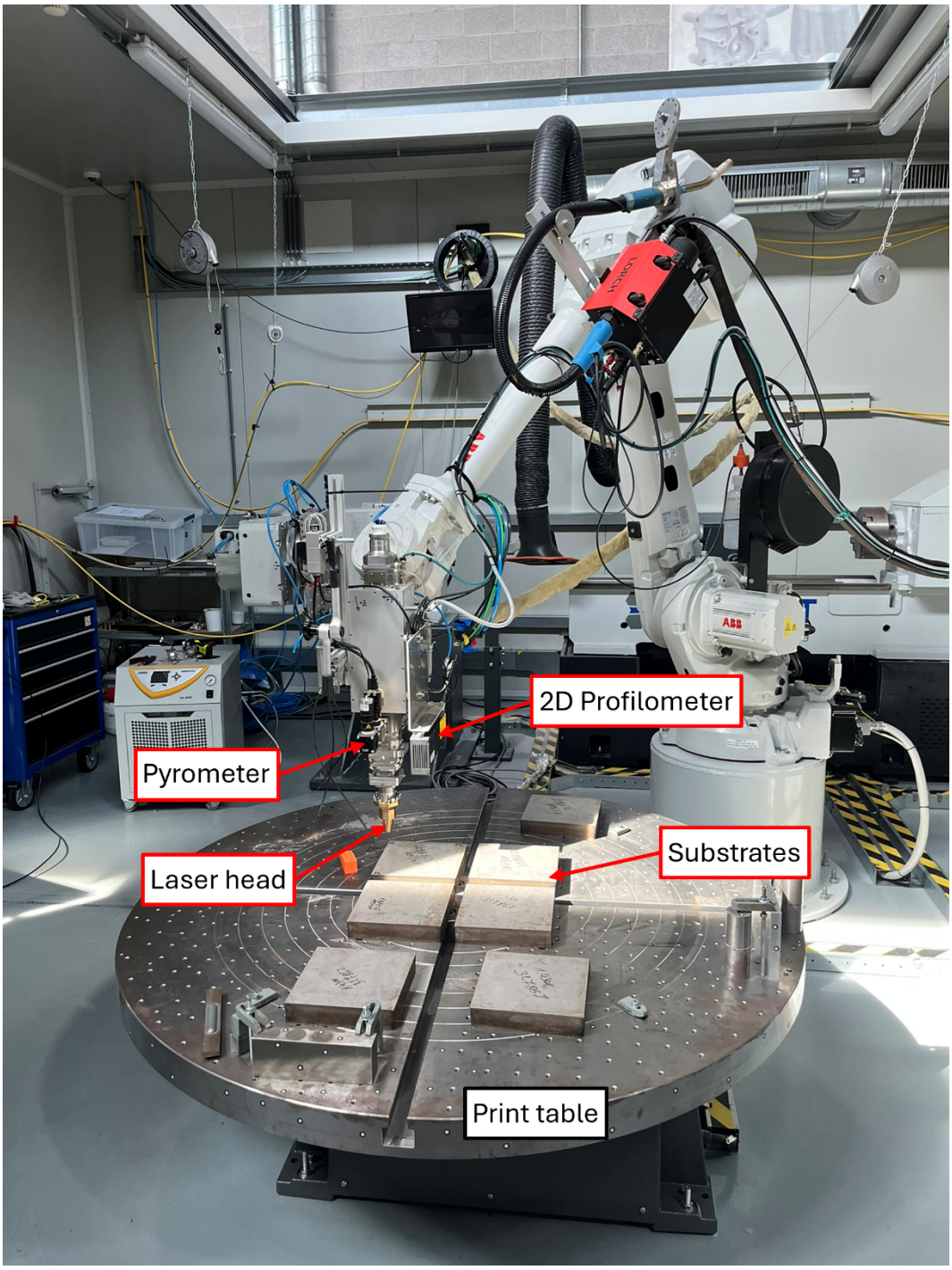


Figure 1. Setup of the on-line detectors in the build environment at CRM Group.

Copyright © by DILAPRO All Rights Reserved | D3.5 - Report on defect detection and classification algorithm for DED-LB

2.1.1 Thermal camera

A FLIR SC7000 thermal camera is used to measure the temperature evolution at the surface of the sample during the print. The camera can be independently positioned to measure various surfaces during the print; for example, at θ = 0 degrees to measure the thermal cycling during printing of multiple layers or at θ > 0 degrees to measure the propagation of heat between adjacent line scans in the same layer. The camera takes off-line measurements and will not be integrated into feedback control of the laser.

Specifications:

- 2 channel temperature measurement
- Temperature range:
  - Channel 1: 180 – 660 °C
  - Channel 2: 540 – 1540 °C
- Mid-wave infrared spectral range : 3.0–5.0 µm
- Resolution : 640x512 pixels
- Frame rate: Programmable, up to ~45 Hz (GigE), 60 Hz (CXP)

Data: Temperature evolution vs. time for points on the sample.

Data Format: Raw data is converted to *.mat files with a matrix of pixel position (xp, yp) and temperature for each point in time. The pixel position can be correlated with the real position (x, y, z) on the printed piece by back-calculation.

Status: Installed, operational

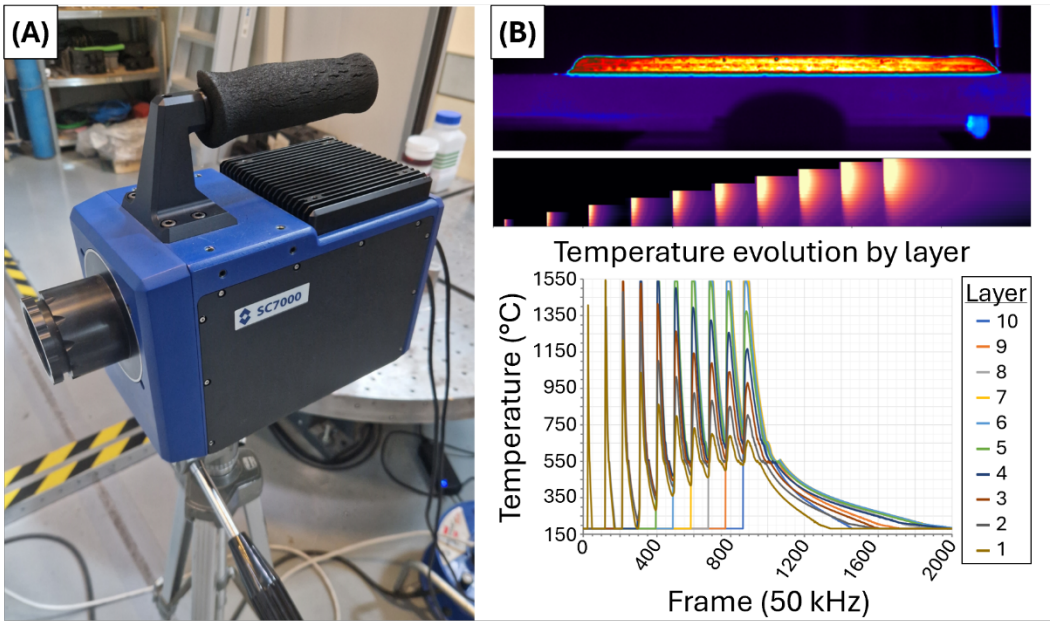


Figure 2. (A) FLIR SC7000 thermal camera. (B) Thermal profile and temperature evolution by layer of a ten-layer print, displayed as a temperature map and numerically.

Copyright © by DILAPRO All Rights Reserved | D3.5 - Report on defect detection and classification algorithm for DED-LB

2.1.2 Laser power and profile monitor

(Previously reported in Deliverable 3.1) A Primes PowerMonitor PM48 and FocusMonitor FM+ are used to measure the power profile of the laser off-line. The measured profile can be correlated with the applied power to 1) model the printing process and 2) operate the laser in de-focused conditions to change the temperature profile, an additional control parameter.

Specifications:

- Power accuracy : ± 3 %
- Reproducibility : ± 1 %

Data: Laser intensity and profile.

Data Format: Matrix of position (x, y) and laser intensity (% of maximum) versus applied power.

Status: Installed, operational

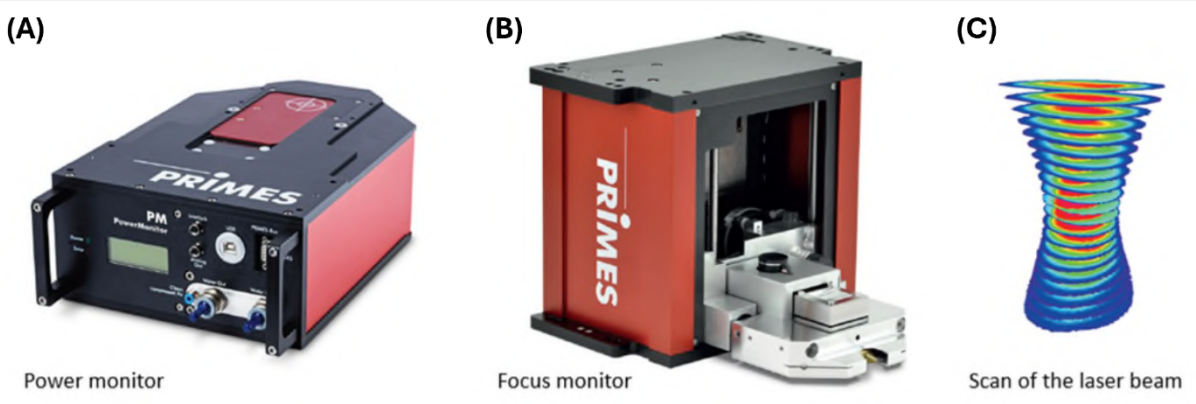


Figure 3. Primes (A) laser power and (B) focus monitor with a (C) digitized scan of an example laser profile. Images adapted from user manual.

2.1.3 Ambient temperature and humidity detector

The ambient temperature and humidity of the printing cabin are measured during the print. Ambient print conditions can be correlated to the build time.

Copyright © by DILAPRO All Rights Reserved

2.2 On-line data acquisition

2.2.1 CLAMIR infrared camera

A CLAMIR infrared (IR) camera will be used to measure the melt pool size and shape during printing. The camera will be mounted in-line with the laser and take IR images along the axis of the laser. Real-time monitoring makes it possible to adjust the process parameters during printing to maintain constant melt pool properties (as in [5], [6]).

Specifications:

- Mid-wave infrared spectral range : 1 µm - 5 µm
- Resolution: 128 x128 pixels
- Frame rate: 2000 fps – 4000 fps
- On- or off-axis positioning

Data: Melt pool size and profile vs. time.

Data Format: Real-time matrix of position (x, y) and temperature along the axis of the laser versus time and power, as well as a single value of width versus time and power.

Status: Not yet installed

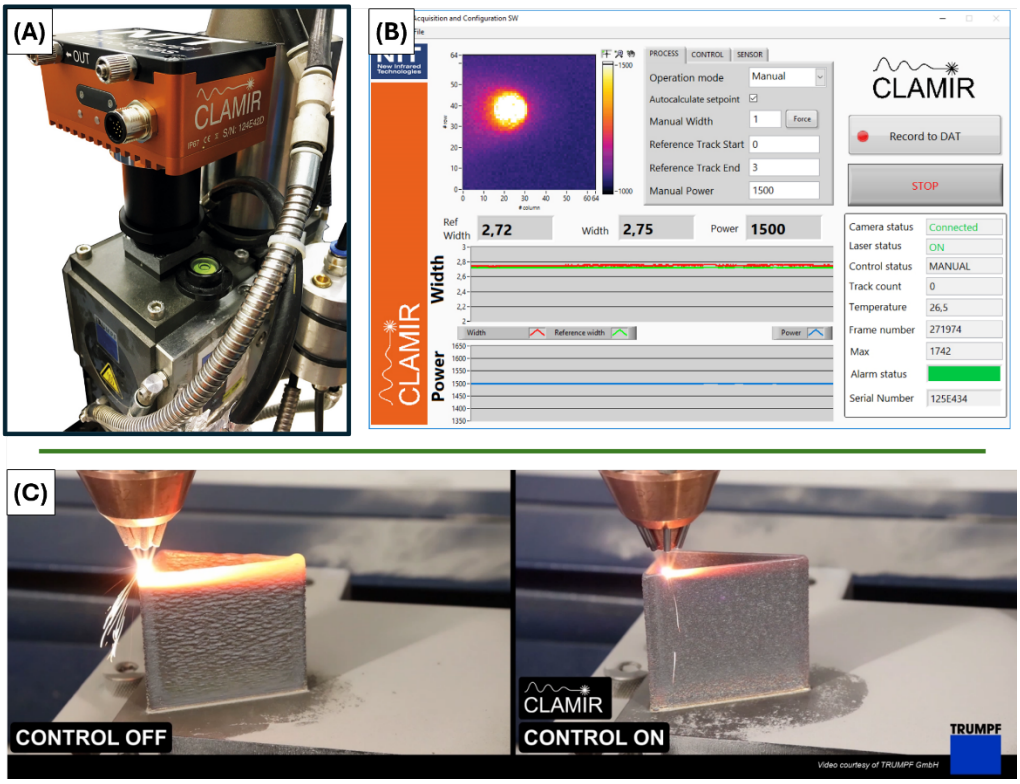


Figure 4. (A) CLAMIR infrared camera and (B) example data acquisition displaying laser spot size and width as a function of power and print time. Images are reproduced from the user manual. (C) Example of live feedback control of melt pool size to improve surface quality and layer homogeneity, courtesy of Trumpf GmbH.

Copyright © by DILAPRO All Rights Reserved | D3.5 - Report on defect detection and classification algorithm for DED-LB

2.2.2 Coaxial pyrometer

A LASCON coaxial pyrometer (Dr. Mergenthaler GmbH) is used to measure the true temperature at the center of the melt pool with high accuracy. The pyrometer is mounted on the laser head and aligned with the laser axis through a series of radiation transparent mirrors. Real-time monitoring makes it possible to adjust the process parameters during printing as a function of the temperature (e.g. in [7]).

Specifications:

- High Speed fiber-coupled 2 Color Pyrometer
- Emissivity filtering
- Temperature range : 800-2200°C
- Measurement frequency : 10 kHz
- Spot diameter : ≥ 100 µm

Data: Temperature at the center of the melt pool vs. time.

Data Format: Raw data *.csv of temperature vs. time. Each comma separated value corresponds to interval +Δt from the start of the print, where the interval can be chosen. Currently, Δt = 500 ms.

Status: Installed, operational

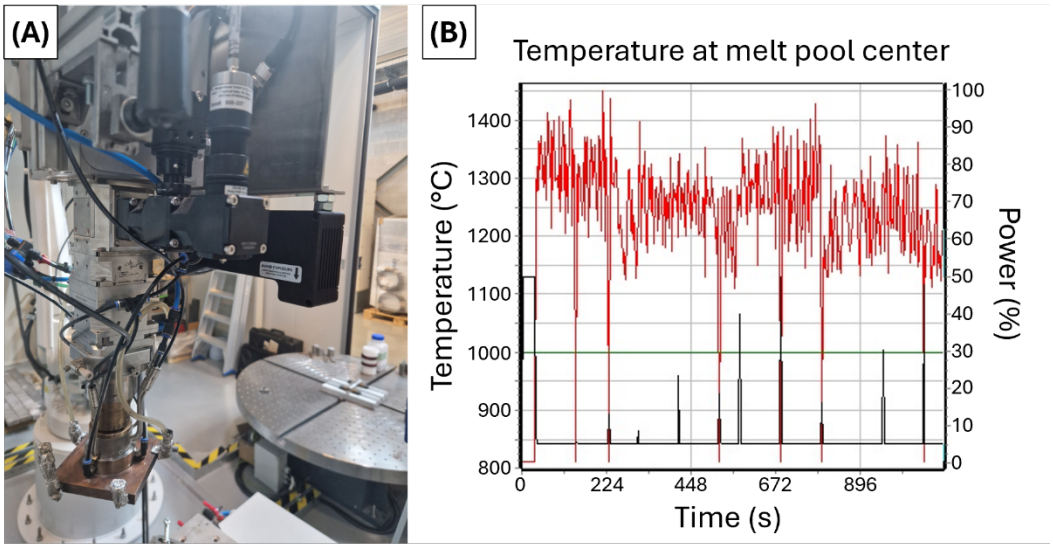


Figure 5. (A) LASCON laser pyrometer and (B) sample temperature versus applied laser power (expressed as a percentage) for the build of an aeronautic component.

2.2.3 2D profilometer

A Gocator 2450A profilometer is used to measure the layer height and roughness during printing. The system is a single line laser scanner that follows the laser print. The profilometer can be operated both on- and off-line. On-line: Profile data from layer N can be used to adjust the parameters for layer N+1, for example if there are variations between the

Copyright © by DILAPRO All Rights Reserved

desired geometry and the actual build. Off-line: The laser can perform multiple scans of the final printed pieces with the same range-of-motion as the laser head to recreate the full print in three dimensions.

Specifications:

- Laser : Blue laser (Class 2, 3R, 3B)
- Data points/profile : 1800 points
- Resolution X : 100 – 255 µm
- Repeatability Z : 2 µm
- Field of view : 145 -425 mm

Data: Height and profile of the printed piece.

Data Format: Initial scan (substrate surface) and final scan (top surface of printed pieces) as a cloud of points in *.csv format. Can be converted and exported as an *.stl. One single scan is taken for the entire part. Therefore, if multiple pieces were printed on the same substrate, the corresponding point clouds must be separated manually.

Status: Installed, operational

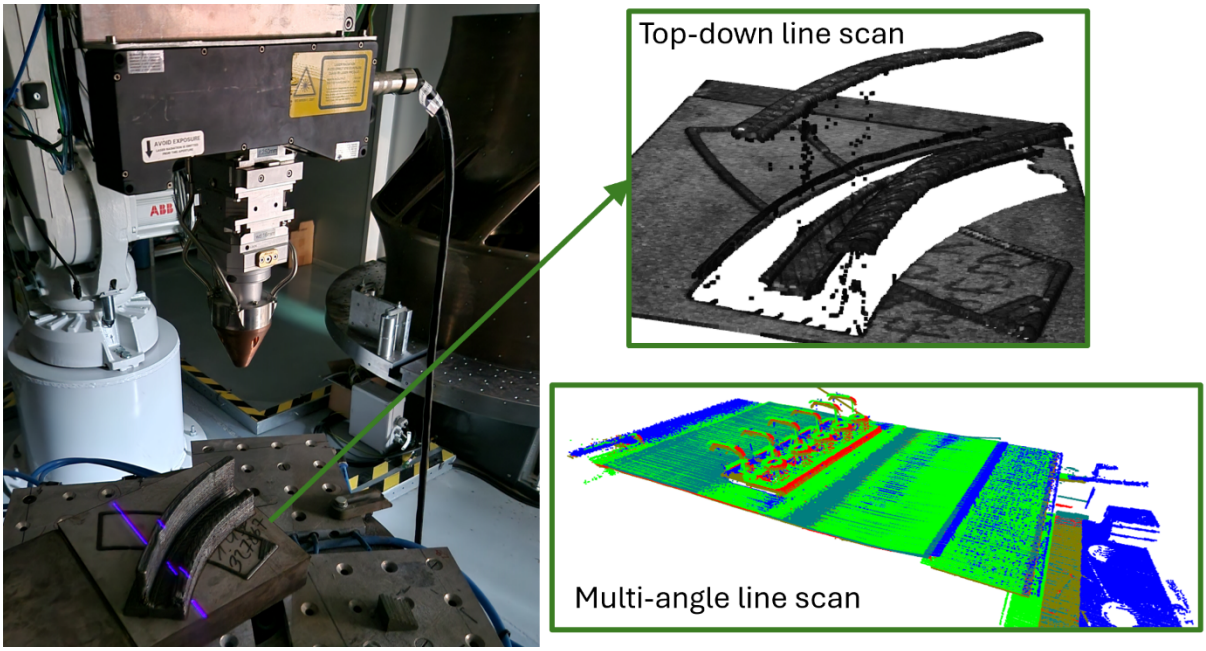


Figure 6. Gocator 2450A line profile sensor with examples of a single-angle, top-down line scan and a three-angle scan, demonstrating the ability to examine a 180 degree field of view above the baseplate.

2.2.4 Eddy Current sensor (Prima Additive)

To enhance in-process quality assurance during Directed Energy Deposition (DED), a new feature has been integrated into the Prima DED laser head on the Prima Additive Laserdyne

Copyright © by DILAPRO All Rights Reserved | D3.5 - Report on defect detection and classification algorithm for DED-LB

811 system. This upgrade enables the installation of eddy current sensors, specifically tailored for porosity and crack detection during the additive manufacturing process. By embedding these sensors within the deposition environment, the system now offers real-time, non-invasive monitoring of material integrity—providing critical insights into defect formation and promoting adaptive control for improved reliability and part performance. This marks a step forward in intelligent, sensor-driven manufacturing within Prima Additive's advanced DED solutions.

Specifications:

- Dimensions (LxWxH): 2800 x 6780 x 3500 mm
- Weight : 9550 kg
- Number of integrated axes : 5 to 7
- Deposition accuracy : ± 0.2 mm / 2 mm
- CAM software (optional) : MasterCam DED

Data: Internal defects (porosity, cracks).

Data Format: Impedance values as *.aimd files.

Status: The integration of eddy current sensors within the Prima DED laser head was validated through a series of structured tests conducted on coupon cubes. These specimens were produced using varying process parameters to simulate a range of deposition conditions and potential defect scenarios.

Sensor performance and consistency were evaluated by conducting layer-by-layer checks at 10, 20, and 30-layer intervals. This approach ensured progressive monitoring of porosity and crack formation throughout the build, allowing us to correlate sensor data with evolving structural integrity. The results have provided valuable insight into the feasibility and reliability of real-time defect detection within the DED environment.

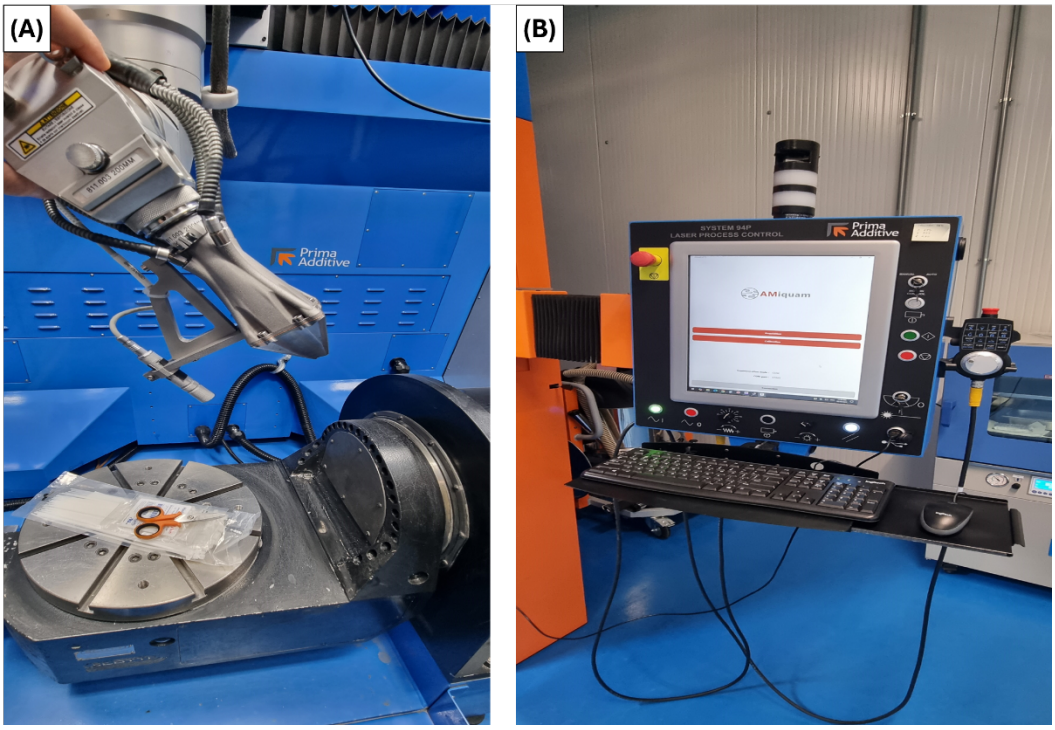


Figure 7. (A) Eddy current sensor and (B) software integration at Prima Additive.

2.3 Defect labeling

Typical defects were detailed in Deliverable D3.1: Analysis of sensors [1]. This section describes how each defect is linked with the installed sensors.

2.3.1 Gas pores

Description: Gas pores are spherical voids that contain gas within the printed solid material. The gas may be entrapped from the environment during printing due to turbulent flow within the melt pool or due to the release of entrapped gas in the powder [8], [9], [10], [11].

In-process detection:

- Direct: Gas porosity can be directly detected with the eddy current sensor. The impedance of the material with respect to an applied alternating magnetic field changes as a function of the local density change due to the formation of a pore.
- Indirect: The melt pool shape and depth are correlated with gas entrapment. Machine learning can determine how gas porosity varies with input from the CLAMIR IR camera, pyrometer, and applied laser power.

Copyright © by DILAPRO All Rights Reserved | D3.5 - Report on defect detection and classification algorithm for DED-LB

2.3.2 Lack of fusion

Description: Lack of fusion detects create irregularly shaped voids due to incompletely melted powder [8], [9], [11].

In-process detection:

- Direct: Lack of fusion voids can be directly detected with the eddy current sensor.
- Indirect: The melt pool shape and depth are correlated with lack of fusion defects. Machine learning can highlight the presence of lack of fusion defects with input from the CLAMIR IR camera, pyrometer, and applied laser power.

2.3.3 Cracks

Description: Hot cracking may occur due to thermal gradients generated during the print. Strong thermal gradients cause adjacent material to expand and contract differently, resulting in cracking. Cracks are known to be exacerbated by compositional differences at the interfaces of grains, which locally changes the coefficient of thermal expansion [8], [9], [12].

In-process detection:

- Direct: Cracks near the surface may be directly detected with the eddy current sensor. However, cracks which form later in the build due to thermal cycling or near the interior of the sample will not be able to be directly detected.
- Indirect: Temperature gradients can be determined live from the FLIR camera and CLAMIR camera IR measurements. The gradients may be used to predict the likelihood of cracking in the interior of the sample.

2.3.4 Thermal distortion and warpage

Description: Thermal gradients generated during the build cause adjacent material to expand and contract differently, leading to inhomogeneous residual stresses. The stresses can either warp the part visibly during the print, or lead to distortions during post-treatment as the residual stresses are removed [8], [9], [12].

In-process detection:

- Direct: Live profilometer scanning can directly measure differences between the desired and actual build.
- Indirect: The thermal history of the part, measured by the FLIR and CLAMIR IR cameras, can be used to predict the development of internal stresses in the part.

2.3.5 Layer height and surface quality (roughness and waviness)

Description: Variations in local cooling and melt pool stability, fluctuations in powder flow rate, and other factors can reduce layer quality [8], [9], [12]. This may manifest as a change in the average height of a layer, e.g. a decrease in the height as the laser head moves further from the baseplate. Within a single layer, it may also cause the surface to become rougher

Copyright © by DILAPRO All Rights Reserved

or wavy, which may provoke more internal defects or cause the final piece to fall outside dimensional tolerances.

In-process detection:

- Direct: Live profilometer scanning can directly measure the quality of the surface layer by layer.
- Indirect: Local changes in layer height will defocus the laser, which causes the melt pool to change. Fluctuations in the melt pool width and temperature can be measured with the CLAMIR IR camera and pyrometer.

2.4 Demonstration of closed-loop control

A closed-loop control system of layer stability has been developed as the first of the on-line defect correction suite. This section describes the algorithm and shows how it can be applied to a real use case: a flight component for the European Space Agency (ESA). The control system uses feedback from the 2D profilometer. Similar closed-loop systems, focused on controlling the density and microstructure, are planned for the other sensors.

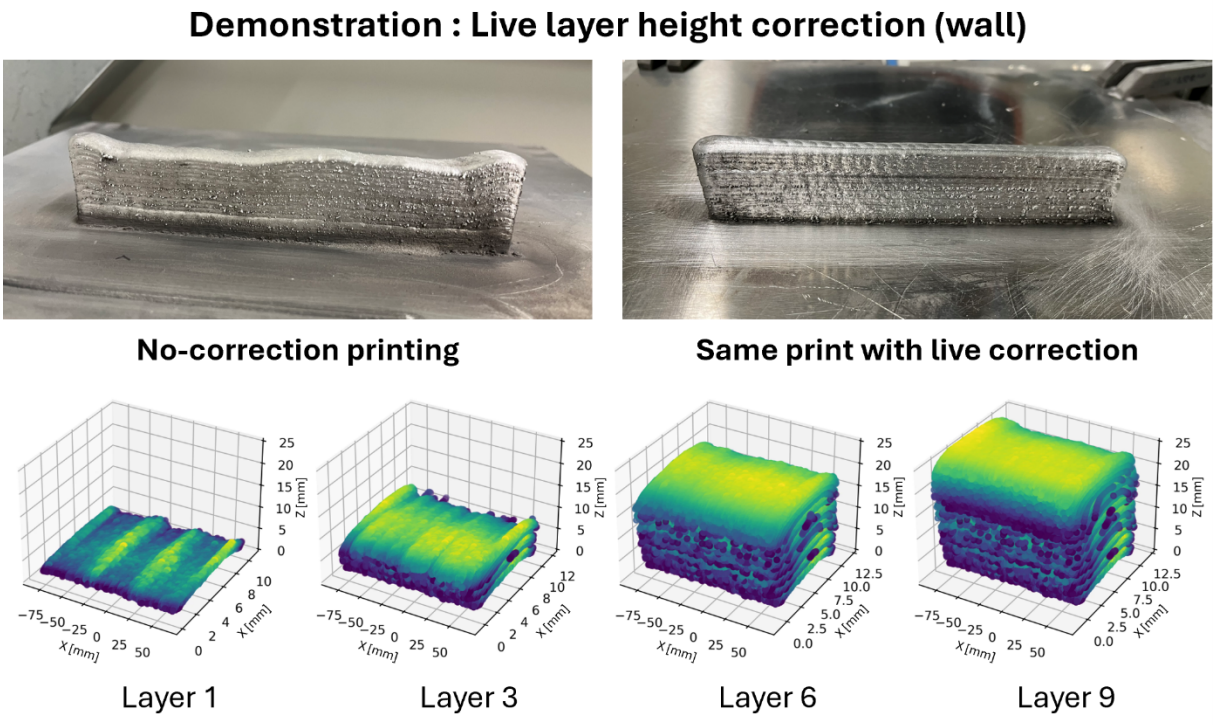


Figure 8. Demonstration of layer height and quality correction by live feedback control of laser power based on profilometer measurements.

Close-loop control has been implemented to stabilize the geometry along the build direction during printing. The algorithm first assesses the geometric accuracy of the current print at layer "N" and a correction is applied for the subsequent layer "N+1". A

Copyright © by DILAPRO All Rights Reserved | D3.5 - Report on defect detection and classification algorithm for DED-LB

demonstration of the layer-by-layer control is shown in Figure 8. The algorithm is described below.

Geometric control:

1. The coordinate system of the tool center point (TCP) of the profilometer is defined.
2. A preliminary scan is launched to establish a reference plane. The scan procedure moves the profilometer along a pre-defined path and sends triggers that register the current position of the TCP and launches a line scan.
    a. This procedure is repeated for each layer (or each group of layers, if layer by lay correction is not necessary) during the print. Currently, the preliminary scan is launched manually, but it can be automated.
3. The data is read as a cloud of points where the X and Z (build direction) positions are measured by the profilometer, and the Y position is obtained from the robotic arm position.
4. For live printing, the cloud of points is trimmed to only account for the last few millimeters printed to reduce computation time. The difference in Z between the trimmed point cloud and the expected tool path points is calculated.

Close loop correction:

1. The difference between the measured and ideal datasets on layer N defines how much the next layer, N+1, should be corrected to achieve planarity and correct layer height.
2. The current algorithm modifies scan speed, powder flow, and laser power for each section of the tool path of the "N+1" layer. The goal is to add more material when the difference is negative, and add less material when the difference is positive.
    a. Currently, the calculation is executed off-line. In other words, the printing process is stopped until the modifications can be calculated and a new print file generated. This can be improved to run without stopping the print.
3. To increase efficiency, and if the part allows, this correction loop can be applied not layer by layer, but every 2, 3, 4... layers. In this case, the total deviation to be corrected is divided by the number of layers being processed.

Copyright © by DILAPRO All Rights Reserved

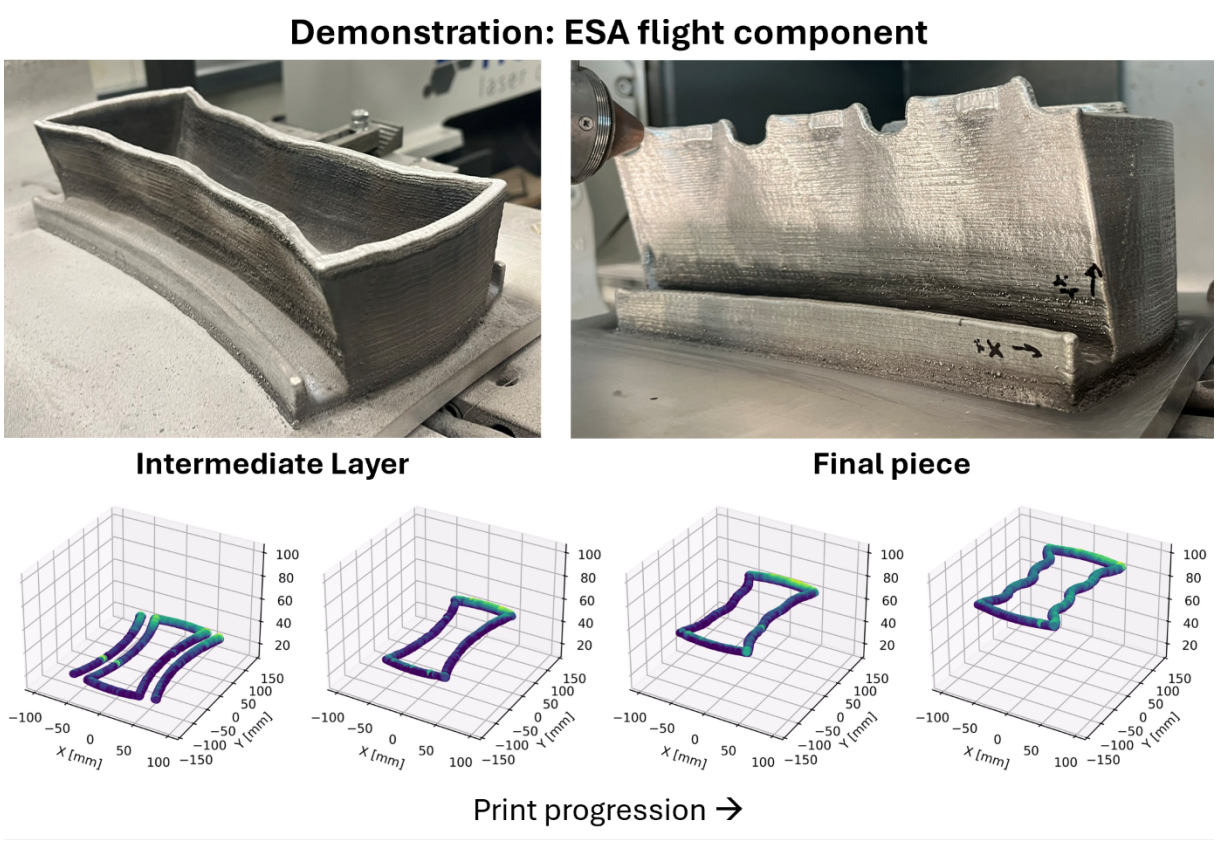


Figure 9. Demonstration of live layer height and quality control used to print a real component.

As a proof-of-concept, the algorithm has been applied to print a flight component for the European Space Agency (ESA), shown in Figure 9. The closed-loop control allows for the part to be printed within the dimensional tolerances of the piece. The next steps for the algorithm are to:

- Automate the preliminary scan.
- Bring the calculation on-line to avoid pauses during the print.
- Incorporate the ML results to ensure that local microstructure is not affected by the changing process parameters.

3. Construction of Machine Learning Dataset

A dataset of process parameters, correlated with their print quality, is necessary to train the machine learning model developed by DCU. To this end, 256 samples of Inconel 718 were printed by DED varying four key process parameters: laser spot size, laser power, scan speed, and line spacing (controlled as percentage overlap between adjacent lines). The values tested are shown in Table 1. All other process parameters were kept the same,

Copyright © by DILAPRO All Rights Reserved | D3.5 - Report on defect detection and classification algorithm for DED-LB

including laser spot profile, powder feed rate and pressure, and scan strategy. All samples were printed under a blanket of Argon.

Table 1. Process parameters tested for the training dataset

Variable process parameter	**Values tested**
Laser spot size (dia.)	1.5, 2.0, 2.5, 4.1 mm
Scan Speed	0.5, 1.0, 1.5, 2.0 mm/min.
Laser power	1000, 1500, 2000, 2500 W
Line overlap (affecting line spacing)	20, 30, 40, 50 %

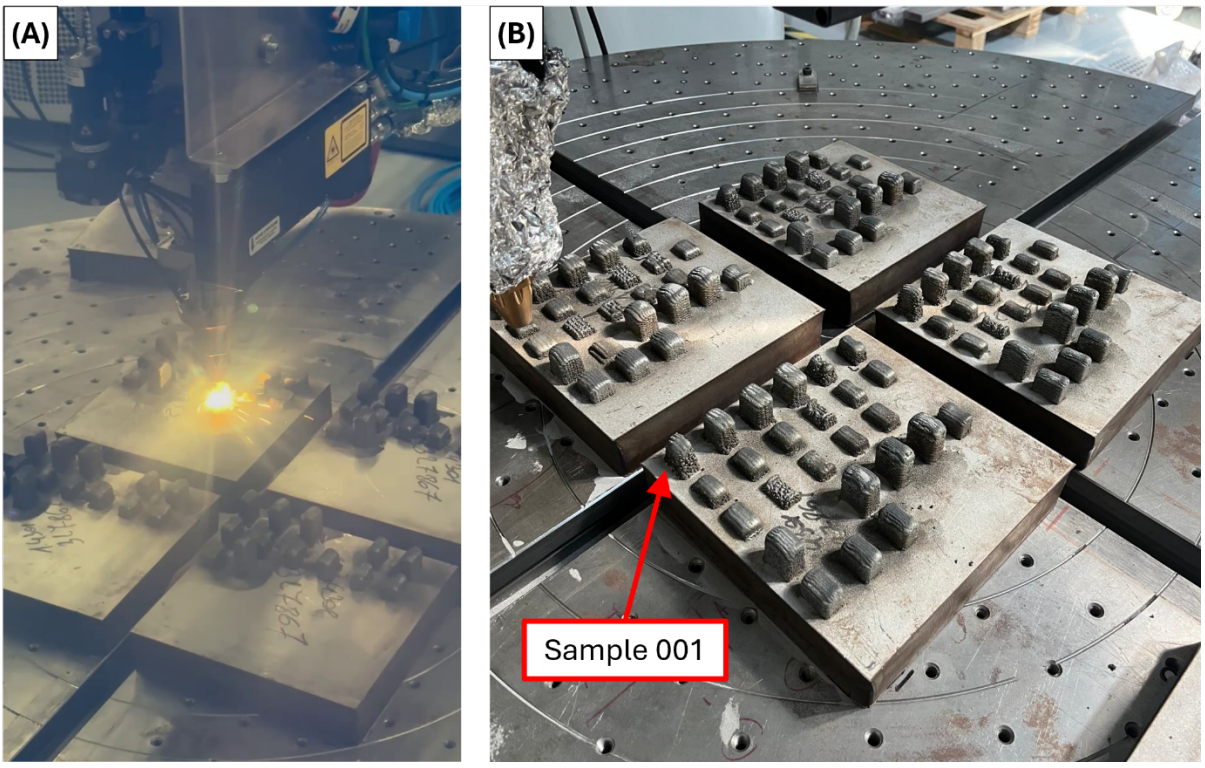


Figure 10. Images (A) during printing and (B) of final printed pieces of the training dataset. Sample 001, used below as an example, is indicated.

Images from the printing of the training data set are shown in Figure 10. The samples were rectangular blocks with nominal dimensions 20 mm × 20 mm and a variable height dependent on the process parameters. Each sample was 20 layers. For each layer, samples were scanned in parallel lines from left to right, with the direction of the scan being rotated 180° on alternating layers. Because the line overlap was one of the process parameters being changed, the number of line scans was adjusted to always maintain a sample width near 20 mm. The vertical displacement of the laser head was kept at a fixed value for each speed, based on experience.

Copyright © by DILAPRO All Rights Reserved | D3.5 - Report on defect detection and classification algorithm for DED-LB

After printing, the samples were removed from the substrate by wire electro-erosion. The density of each sample is measured by pycnometry in an Ultrapyc 5000 (Anton Paar) with Helium gas.

After the density of each sample was measured, a section of each sample was cut perpendicularly across the scan direction, again by wire electro-erosion. The sample surface was polished to mirror finish to measure the hardness. Hardness was measured as the average of up to 5 points (depending on the size of the sample) taken by Vickers indenter with a load of 1 kg, hold duration 15 seconds. These measurements are ongoing.

3.1 Live sensor data

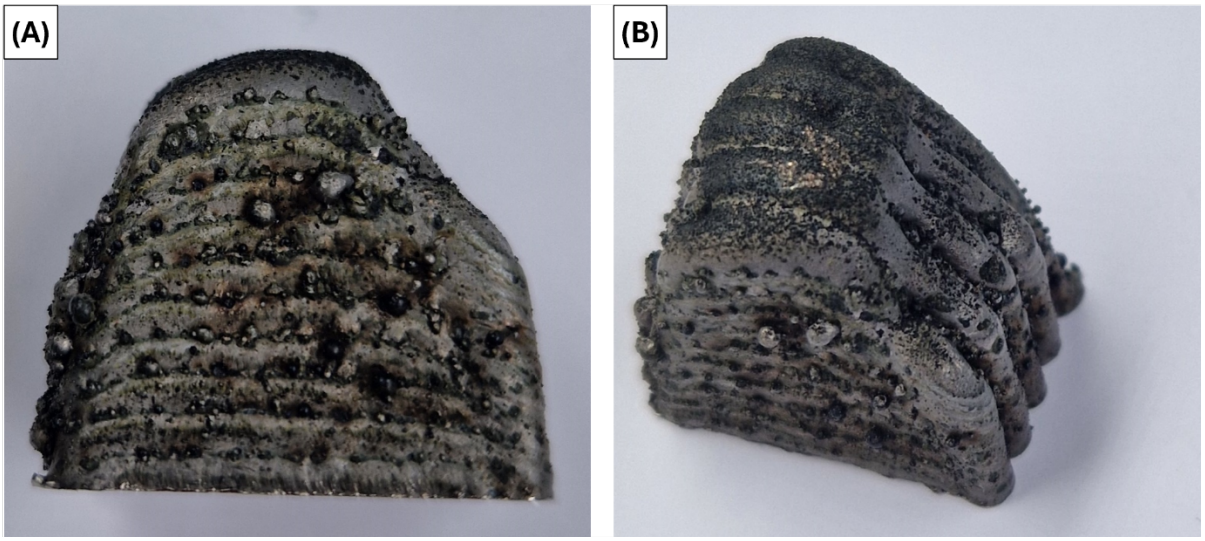


Figure 11. Optical images of Sample 001 after its removal from the baseplate. (A) Image along axis perpendicular to the build direction. (B) Isometric view.

The following section shows an example of the sensor data collected for Sample 001 of the dataset, shown in Figure 11. The same data was collected for all 256 samples in the training dataset. As seen from the final images, the sample varied greatly from the expected 20 × 20 mm^2 cross section after a few layers. The surface shows signs of burning and redeposited spatter in the form of small spheres of melted powder.

Copyright © by DILAPRO All Rights Reserved | D3.5 - Report on defect detection and classification algorithm for DED-LB

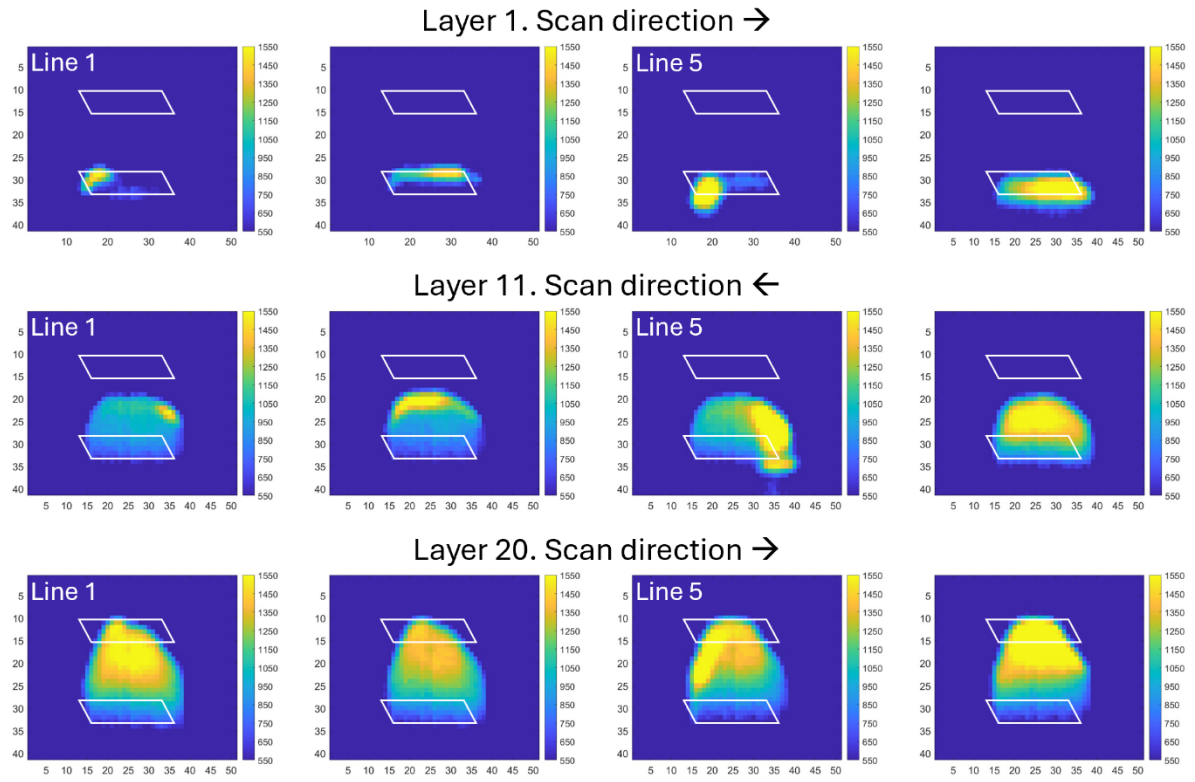


Figure 12. FLIR thermal camera data of selected frames for Sample 001. Evolution of temperature profile versus time. The white boxes serve as a guide to the eye for the positioning of the sample in 3D space.

The thermal history on the surface of Sample 001 was measured by the FLIR SC7000 thermal camera during printing. The results are visualized in Figure 12. The camera was mounted at ~20 degrees to the sample, so two temperature profiles can be calculated. One measures the thermal cycling due to subsequent laser scans within the same layer. The second is the temperature evolution on the side wall, which shows the thermal cycling induced by subsequent layers. Each sample has a slightly different position and thus angle with respect to the thermal camera. The coordinates of each pixel must thus be back-calculated for each sample based on the specific vector tracing between the camera lens and the sample.

Copyright © by DILAPRO All Rights Reserved | D3.5 - Report on defect detection and classification algorithm for DED-LB

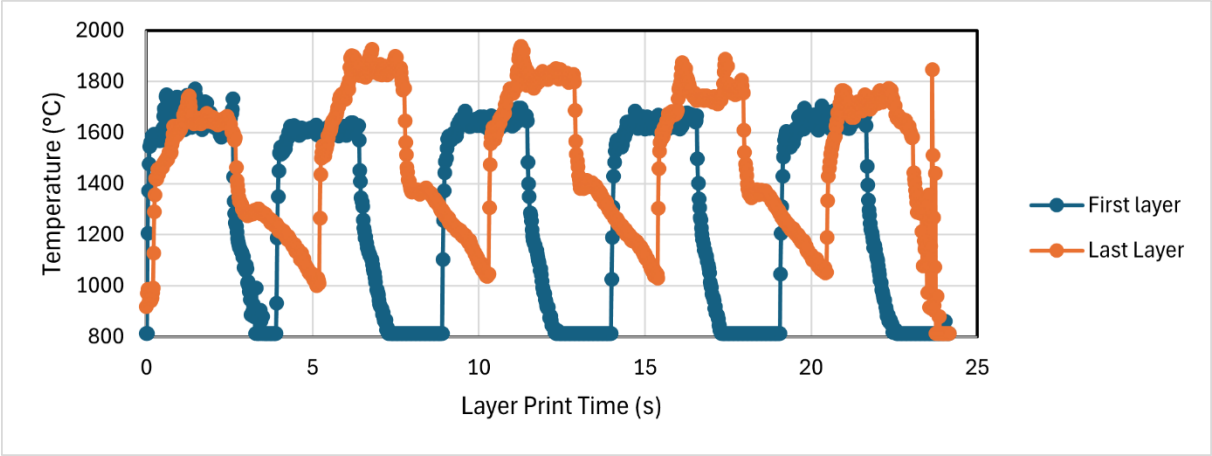


Figure 13. Coaxial pyrometer data for the first and last layer of Sample 001.

The thermal history of the melt pool of Sample 001 was measured by the pyrometer during printing. The temperature evolution during the first and last layer are shown in Figure 13. The lower limit of the sensor is capped at 811.7 °C. The ideal steady-state pattern would resemble a rectangular waveform, with a constant maximum temperature while the laser is illuminated. Even in the first layer, however, there is a "tail" at the end of each crest caused by the pyrometer measuring residual heat build-up as the print head moves back towards the beginning of the line to print the next line. By the end of the print, the rectangular waveform is lost due to the irregular shape of the top layer. It is also noteworthy that the pyrometer never reads below 1000 °C as it repositions for a new line. The residual heat in the sample, as well as the larger distance from the cooled baseplate, have reduced the cooling rate at the surface of the sample. This data can be used to reconstruct a thermal history of the temperature in the melt pool, layer-by-layer, and adjust it during the build.

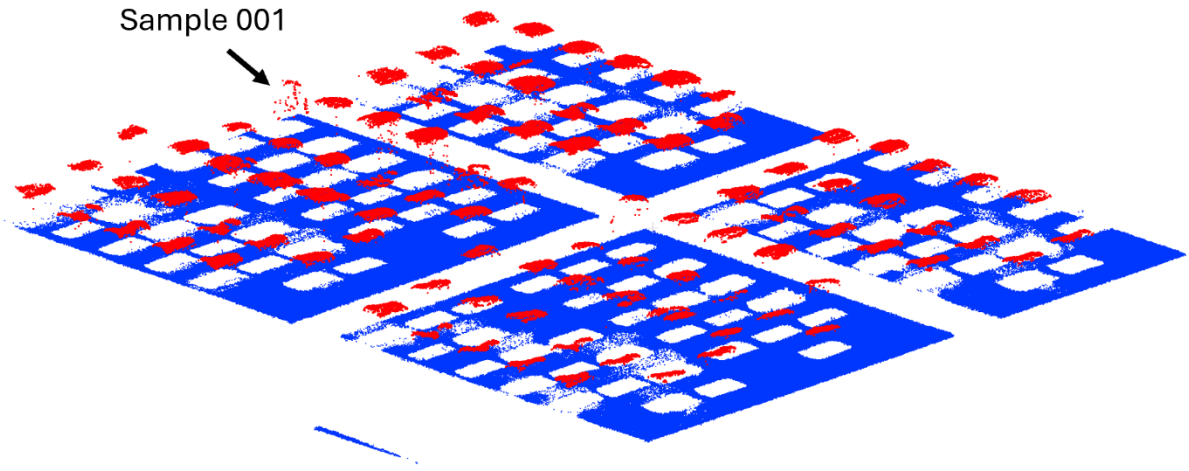


Figure 14. 2D profilometer scan after printing, shown as a cloud of points. Blue points are the substrate, red points are the top surfaces of the printed samples.

Copyright © by DILAPRO All Rights Reserved | D3.5 - Report on defect detection and classification algorithm for DED-LB

The final profilometer scan after one of the training set prints is shown in Figure 14. Sample 001 is indicated with a black arrow. The blue layer shows the tops of the baseplates, while the red layer shows the tops of individual samples. The difference in Z (build direction) between the red points and the plane of the baseplate defines the height of the sample. The points measured on the surface of the sample can also be used to quantify the "planarity", or the deviation from a perfect plane, of the total layer of the sample. This can be used as an additional quality measurement for the machine learning algorithm.

4. Classification Algorithm

Potential Inputs:

1. Temperature at the center of the melt pool (the point of contact with the laser on the surface) for every point (x,y,z) on the sample. Data from pyrometer.
2. Complete evolution of temperature vs time for every point on one wall of the piece. T vs t for each point (x fixed, y, z). Data from FLIR thermal camera.
3. Final surface of the printed block as a cloud of points. (x, y, z-z0) for top layer, where z-z0 is the height above the substrate. Final dimensions length, width, height, and a quantification of planarity (average distance of points from average surface?). Data from 2d profilometer.
4. Melt pool width for each point (x, y, z) at moment of fabrication. Data from CLAMIR IR camera.*

*The CLAMIR camera is not yet available so this data will not be included in the first version of the model.

Potential quality measurements:

1. Relative density of part. Measured by pycnometer.
2. Relative hardness of part (absolute magnitude of distance from desired value).
3. Over soft or over hard. Binary value of whether hardness is above or below desired value.
4. Dimensional variation of the final part from the desired part.
5. Microstructural features: grain size and distribution, morphology, preferred orientation (texture)**

**These values are for future versions of the model and will not be implemented during the Dilapro project. The Dilapro algorithm will focus on full part density and dimensional conformity.

Copyright © by DILAPRO All Rights Reserved

4.1 Criteria for defect classification

The criteria for defect classification in Deliverable D3.5 are based on the defect detection strategy introduced in Deliverable D3.4 [4], Section 3. This approach employs a sigmoid transformation of relative density values to convert continuous regression outputs—specifically, machine learning predictions of relative density—into probabilistic indicators of defect presence.

For a detailed explanation of using relative density as a defect indicator, please refer to Section 2.1 of Deliverable D3.4 [4]. In brief, relative density is widely accepted as a key quality metric in additive manufacturing, as it measures the proportion of solid material in a printed part. Lower relative density values are typically associated with internal voids or defects, making it a suitable basis for defect classification.

The probability that a given layer is defective ($P_{(defect)}$), is calculated using the following modified sigmoid function [13]:

$$P_{(defect)} = \frac{1}{1+e^{(x-98)}} \quad (1)$$

In line with the criteria established in Deliverable D3.4 [4], the relative density threshold $\boldsymbol{x_0}$ = 98% and steepness parameter $\boldsymbol{k}$ of -1 were adopted. As a result, predictions of relative density significantly below 98% correspond to a higher probability of defect presence, whereas values above this threshold are increasingly associated with reliable, defect-free regions.

4.2 Model Training and Selection Criteria

Multiple regression algorithms similar to those described in Deliverable D3.3 and D3.4 will be explored using the a similar methodology also described in Deliverable D3.3 [2], [4]. The key difference in this Deliverable D3.5 task lies in the choice of predictive features—specifically, sensor data described in Sections 1 through 3 of this document—which will require an iterative process of feature engineering and selection. This process aims to identify the most informative set of sensor features that can deliver high predictive accuracy while minimizing computational overhead and model complexity.

The objective is to train these models to predict the sigmoid-transformed relative density of the Inconel 718 samples printed by DED. The best-performing model will then be selected based on based on its ability to satisfy the established performance criteria described in Deliverable D3.3 [2]. This includes:

1. Predictive Accuracy based on R^2 score during exploratory training phases.
2. Performance consistency based on mean R^2 across multiple cross-validation folds.
3. Lower Bound of True Performance during cross-validation 95% confidence interval.

Copyright © by DILAPRO All Rights Reserved | D3.5 - Report on defect detection and classification algorithm for DED-LB

4. Performance Superiority in at least two of the following performance metrics:
    a. Mean Squared Error (MSE)
    b. Root Mean Squared Error (RMSE)
    c. Mean Absolute Error (MAE)
    d. Mean Absolute Percentage Error (MAPE)

5. Conclusion

Deliverable D3.5 reports the progress on defect detection during DED printing and the development of a classification algorithm for predicting defects. The following sensors have been integrated on the machine:

- LASCON coaxial pyrometer (measure temperature at center of melt pool)
- FLIR thermal camera (temperature evolution at the surface of the print)
- Gocator 2450A 2D profilometer (2d in-line layer geometry data, 3D final dimension data of printed part)
- Laser power and profile monitor (laser intensity and profile with respect to applied power)

The following sensors are still being integrated into the machine:

- CLAMIR IR camera (monitoring of melt pool size and profile)

A dataset of 256 samples has been printed in Inconel 718 to train the machine learning model. For each sample, the following data was measured during printing: thermal profile of each layer and one side wall, melt pool temperature, and geometry of the final surface (dimensions, planarity). Due to delays in the reception and installation of the sensors, the samples are still being characterized. Relative density, hardness, and dimensional accuracy may be used in the algorithm to quantify the quality of the printed samples. This may be extended later to more microstructural properties.

The next step is to train and evaluate the machine learning model. Additional data will be furnished as needed. Once an acceptable performance is achieved, the model may be used to create in-line monitoring and control of process parameters. The model will also be mined for previously undiscovered correlations between parameters and print quality.

Copyright © by DILAPRO All Rights Reserved | D3.5 - Report on defect detection and classification algorithm for DED-LB

6. References

[1] DILAPRO, "Deliverable D3.1: Analysis of sensors and identification of technical solutions," CRM Group, 2024.

[2] DILAPRO, "Deliverable D3.3: Report on Real-time Feedback Control Algorithm.," Dublin City University, 2025.

[3] A. Phua, C. H. J. Davies, and G. W. Delaney, "A digital twin hierarchy for metal additive manufacturing," *Computers in Industry*, vol. 140, p. 103667, Sep. 2022, doi: 10.1016/j.compind.2022.103667.

[4] DILAPRO, "Deliverable D3.4 Report on Defect Detection and Classification Algorithm for PBF-LB," Dublin City University, 2025.

[5] B. T. Gibson *et al.*, "Melt pool size control through multiple closed-loop modalities in laser-wire directed energy deposition of Ti-6Al-4V," *Additive Manufacturing*, vol. 32, p. 100993, Mar. 2020, doi: 10.1016/j.addma.2019.100993.

[6] V. Pandiyan, D. Cui, R. A. Richter, A. Parrilli, and M. Leparoux, "Real-time monitoring and quality assurance for laser-based directed energy deposition: integrating co-axial imaging and self-supervised deep learning framework," *J Intell Manuf*, vol. 36, no. 2, pp. 909–933, Feb. 2025, doi: 10.1007/s10845-023-02279-x.

[7] Z. Smoqi *et al.*, "Closed-loop control of meltpool temperature in directed energy deposition," *Materials & Design*, vol. 215, p. 110508, Mar. 2022, doi: 10.1016/j.matdes.2022.110508.

[8] D. Svetlizky *et al.*, "Directed energy deposition (DED) additive manufacturing: Physical characteristics, defects, challenges and applications," *Materials Today*, vol. 49, pp. 271–295, Oct. 2021, doi: 10.1016/j.mattod.2021.03.020.

[9] M. Liu, A. Kumar, S. Bukkapatnam, and M. Kuttolamadom, "A Review of the Anomalies in Directed Energy Deposition (DED) Processes & Potential Solutions - Part Quality & Defects," *Procedia Manufacturing*, vol. 53, pp. 507–518, Jan. 2021, doi: 10.1016/j.promfg.2021.06.093.

[10] K. Zhang *et al.*, "Pore evolution mechanisms during directed energy deposition additive manufacturing," *Nat Commun*, vol. 15, no. 1, p. 1715, Feb. 2024, doi: 10.1038/s41467-024-45913-9.

[11] Y. Chen *et al.*, "In situ and Operando X-ray Imaging of Directed Energy Deposition Additive Manufacturing," Jun. 16, 2020, *arXiv*: arXiv:2006.09087. doi: 10.48550/arXiv.2006.09087.

[12] L. Qin, K. Wang, X. Li, S. Zhou, and G. Yang, "Review of the Formation Mechanisms and Control Methods of Geometrical Defects in Laser Deposition Manufacturing," *Chinese Journal of Mechanical Engineering: Additive Manufacturing Frontiers*, vol. 1, no. 4, p. 100052, Dec. 2022, doi: 10.1016/j.cjmeam.2022.100052.

[13] A. Alivanoglou and A. Likas, "Probabilistic Models Based on the Π-Sigmoid Distribution," in *Artificial Neural Networks in Pattern Recognition*, L. Prevost, S. Marinai, and F. Schwenker, Eds., Berlin, Heidelberg: Springer, 2008, pp. 36–43. doi: 10.1007/978-3-540-69939-2_4.

Copyright © by DILAPRO All Rights Reserved